

SPATIAL DISTRIBUTION OF ODORS IN SIMULATED BENTHIC BOUNDARY LAYER FLOWS

PAUL A. MOORE,^{1,3*} MARC J. WEISSBURG,²
J. MICHAEL PARRISH,³ RICHARD K. ZIMMER-FAUST,⁴
and GREG A. GERHARDT³

¹*Monell Chemical Senses Center
3500 Market Street, Philadelphia, Pennsylvania 19104*

²*Department of Biology, Georgia State University
P.O. Box 4010, Atlanta, Georgia 30302-4010*

³*Departments of Pharmacology and Psychiatry
Neuroscience Training Program, and
Rocky Mountain Center for Sensor Technology
University of Colorado Health Sciences Center
Denver, Colorado 80262*

⁴*Department of Biology, Marine Sciences Program, and
Belle W. Baruch Institute for Marine Biology and Coastal Research
University of South Carolina,
Columbia, South Carolina 29208*

(Received June 23, 1993; accepted September 20, 1993)

Abstract—Many animals orient to odor sources in aquatic habitats where different flows and substrates affect the hydrodynamics of benthic boundary layers. Since the dispersal of chemicals is due to the fluid mechanics of a particular environment, we quantified the changes in the fine structure of an odor plume under different hydrodynamic conditions in the benthic boundary layer of a laboratory flume. We sampled turbulent odor plumes at 10 Hz using a microchemical sensor (150 μm diameter) under two flow speeds: 3.8 and 14.4 cm/sec, and at 1, 8, 50 mm above the substrate. These distances above the substrate occur within different flow regions of the boundary layer and correlate with the location of crustacean chemosensory appendages within boundary layer flows. The high flow velocity exhibited a greater level of turbulence and had more discrete odor pulses than the low flow velocity. In general, odor signals showed a high level of temporal variation in fast flow at heights 1 and 8 mm above the substrate. In slow flow, temporal variation was maximal at 50 mm above the substrate, exhibiting more variance than the same height at the fast flow. These patterns of odor signals resulted in

*To whom correspondence should be addressed.

part from differences in the height above the substrate of the main axis of the odor plume at the two flow speeds. Our results imply that animals chemically orienting to an odor source will need to compensate for varying hydrodynamic properties of odor transport and dispersal. The method by which animals extract spatial information from odor plumes will need to account for changing flow conditions, or else it will not be equally efficient in extracting information about chemical spatial distributions.

Key Words—Odor plume, chemical orientation, chemoreception, turbulence, hydrodynamics, electrochemistry, benthic boundary layer, flume.

INTRODUCTION

Odor concentrations in plumes are heterogeneous when measured at fast temporal and small spatial scales (Murlis and Jones, 1981; Atema, 1985; Moore and Atema, 1988, 1991; Zimmer-Faust et al., 1988; Murlis et al., 1991; Moore et al., 1992). The patchy structure of odor plumes is due to turbulence produced by the mechanical forces acting on a moving fluid. The magnitude of concentration fluctuations is dependent on the interaction between the size of the turbulent eddies and the size of the odor plume. This size dependency implies that estimates of odor concentration are determined in part by the temporal and spatial sampling scale of the chemical measurements (Aylor, 1976; Aylor et al., 1976; Miksad and Kittredge, 1979). As a result of this turbulence, animals located downcurrent of an odor source will experience periods during which odor concentrations are well above or below the mean odor concentration and which exhibit unpredictable temporal variation. Thus, mean concentrations and time-averaged distributions (i.e., 5–10 min) may not be indicative of the information available for many macroscopic animals attempting to orient towards an odor source (Elkinton et al., 1984; Moore and Atema, 1988, 1991; Zimmer-Faust et al., 1988; Zimmer-Faust, 1989).

The physical forces governing odor dispersal will depend on the flow regime into which the chemical stimulus is introduced (for review see Westerberg, 1991). Odor transport is influenced significantly by the interaction between a moving fluid (air or water) and a solid surface, such as when air flows over the earth's surface or water flows over the sea floor. The interface between a stationary solid and a moving fluid is called a boundary layer and is a region through which fluid velocities steadily increase as one moves away from the solid surface.

The boundary layer is generally divided into three regions, each of which is characterized by a particular combination of physical forces affecting chemical signal transmission. The region immediately above the solid surface is called the bed layer and actually consists of two sublayers (Wright, 1989). The sublayer closest to the surface (diffusive sublayer) may be only micrometers thick and is

characterized by a near absence of flow. The dispersion of chemicals in this sublayer occurs largely by molecular diffusion. The sublayer further away (viscous sublayer) is characterized by quasilaminar flow, but is dominated by viscous forces tending to dampen turbulence (Wright, 1989). The second region, still further away from the surface, accounts for about 30% of the boundary layer and is called the buffer zone or log layer. This region derives its name from the fact that flow velocity through the log layer is a function of the logarithmic distance above the solid surface. In the log layer, both viscous and inertial forces are important in maintaining the pattern of flow. It is here that small, energetic turbulent eddies are generated when energy associated with the momentum of the advection component of flow is converted to energy associated with eddies. The final, most distant region of the boundary layer is called the outer layer or log-deficit layer. Here, flow is nearly independent of the frictional force imposed by the solid surface on the moving fluid and is characterized by the presence of relatively large turbulent eddies.

Boundary layer flows over any solid object or substrate are often characterized by determining frictional or shear velocity (u_*), and roughness Reynolds number (Re_*). Frictional velocity is a measure of the strength and correlation of turbulent fluctuations in velocity near the substratum. The magnitude of u_* is proportional to the magnitude of eddy diffusivity in a turbulent boundary layer (Fischer et al., 1979). As shear velocity increases, greater eddy diffusion will result in greater dilution and, hence, lower time-averaged concentrations of odorants suspended in the fluid. However, the increased momentum fluxes responsible for eddy generation will also increase the temporal and spatial variation in odor concentration as odorants become entrained in coherent eddy structures. The Re_* provides a means for describing the distance to which turbulent eddies penetrate the boundary layer. As Re_* increases, the effect of turbulence is felt closer to the solid surface. The onset of turbulence in the outer reaches of the boundary layer over a seabed occurs at Re_* between 3.5 and 6 (Nowell and Jumars, 1984; Denny, 1988). Boundary layer flow is fully turbulent (i.e., the turbulence extends all the way to the substrate) when $Re_* > 75-100$.

The turbulence properties of odor dispersal in boundary layers vary with physical environmental conditions, especially substrate type, flow speed, and kinematic viscosity of the fluid. Yet, terrestrial and aquatic animals show the remarkable ability to use chemical signals in orienting to odor sources under a variety of flow conditions (for review see Bell and Tobin, 1982). Many benthic aquatic animals (e.g., decapod crustaceans and fishes) sample chemical signals and orient to plumes using receptor organs located on different parts of the body (McLeese, 1973; Reeder and Ache, 1980; Johnsen and Teeter, 1980; Devine and Atema, 1982). These receptor organs, which are located at different heights above the substrate, should receive different patterns of chemical stimulation from an odor source.

Previous studies have shown that chemical dispersal processes create spatial patterns of odor that could serve as directional cues (Murlis and Jones, 1981; Moore and Atema, 1988, 1991; Zimmer-Faust et al., 1988; Murlis et al., 1991) and that chemoreceptor appendages and cells have temporal filter properties that could serve to further enhance spatial differences in odor plumes (Moore and Atema, 1988). In order to apply the results from these studies to different environments, it is necessary to correlate patterns in the spatial distribution of odors with the physical properties of the fluid environment. Our current study was designed to quantitatively describe aquatic odor plumes emanating from a biologically relevant source in two different flow regimes. Hydrodynamic measurements were made in benthic boundary layers at three different heights above the sediment bed, corresponding roughly to positions within the viscous sub-layer, log layer, and log-deficit layer. The spatial and temporal sampling scale of our chemical measurements were matched to those scales associated with benthic crustacean chemoreception. Our study experimentally demonstrates the critical importance of benthic boundary layer hydrodynamics to the spatial distribution of chemical signals.

METHODS AND MATERIALS

Flume Design and Flow Regime Calculations

Experiments were conducted in steady flows and fully developed turbulent boundary layers within a single-channel, recirculating flume ($10 \times 0.75 \times 0.15$ m; length \times width \times height). The working section, a fixed drop box ($1 \times 0.45 \times 0.15$ m; Figure 1), was placed 7.5 m downstream of the entry section

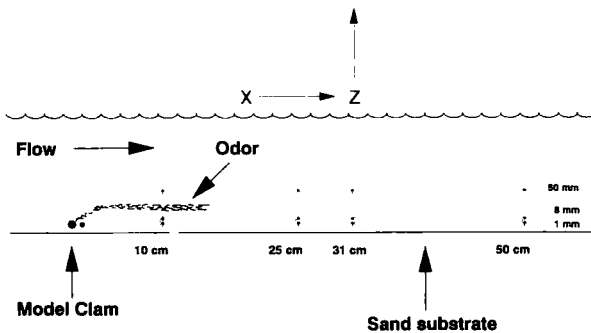


FIG. 1. Diagram showing the working section of the flume used in simulating flows of a benthic boundary layer. Flow was from left to right. Closed circle: model clam. Asterisks: sampling sites. The 75- and 100-cm sites are not shown.

and 1.5 m upstream of the exit weir. The drop box was filled with sand taken from local habitats and sieved to < 1 mm to remove large particles (mean diameter of sand particles: $350 \pm 10 \mu\text{m}$; $N = 100$). The entire flume bed was carefully layered to a uniform depth of 0.5 cm with this material. The dimensions, placement of the working section, configuration of the upwelling section, and baffle arrangements were based on accepted principles of flume design (e.g., Nowell and Jumars, 1987) and ensured that flow through the test section was free from artifacts produced by improper flume architecture. Water exiting the flume was pumped through a $5\text{-}\mu\text{m}$ particle filter, activated charcoal bed, and a UV sterilization unit before being returned. Water salinity was 25 ppt and temperature was $25 \pm 1^\circ\text{C}$. Further details pertaining to the flume are presented in Weissburg and Zimmer-Faust (1993).

Hydrodynamic Measurements

The friction velocity (u_*) and roughness Reynolds number (Re_*) of water flowing through the working section of the flume were determined by measuring the vertical velocity gradient within the log layer. The vertical velocity gradient was characterized by determining the speed of neutrally buoyant particles injected at known heights above the substrate, a technique similar to that used by Ertman and Jumars (1988). Black styrene-divinylbenzene particles ($350 \mu\text{m}$ diameter, specific gravity 1.03 g/ml; Bangs Laboratories, Carmel, Indiana) were injected isokinetically using a variable-speed syringe pump and microcapillary tubing (ID 1.1 mm, OD 1.4 mm) with the tube tip oriented parallel to the flow. The length of the capillary tube arm parallel to the flow was approximately 2 mm. The delivery tube was affixed to a three-dimensional micromanipulator that allowed precise spatial positioning of the tube. Velocity profiles were determined over at least five heights in the log layer, a necessary condition for accurate measurement of boundary shear velocities (Nowell and Jumars, 1984, 1987).

Particle trajectories were recorded on video tape for later motion analysis of velocity. The field of view was 2×2 cm and began 15 cm downstream from the tip of the delivery tube. At this distance ($50\times$ the length of the tube's projection into the flow), particles entering the field of view were free from the flow effects generated by the delivery tube. The velocity of 25 particles was determined on a frame-by-frame basis over 10–20 video frames. Thus, an average of 250–500 particle velocity realizations were determined for each height above the substrate. Full details on motion analysis of bead trajectories are described elsewhere (Weissburg and Zimmer-Faust, 1993). Velocity measurements based on particle trajectories and motion analysis were confirmed by making velocity determinations in some instances with a hot bead thermistor probe (LaBarbera and Vogel, 1976; as modified by M. Patterson and M.L. Judge).

The vertical velocity profiles provided data that allowed us to use the "Law of the Wall" in calculating shear velocity as:

$$U_z = \frac{u_*}{\kappa} \ln \left(\frac{z}{z_0} \right) \quad (1)$$

where U_z is the mean velocity at height z above the bed and κ is von Karman's constant (0.41). The hydraulic roughness length (z_0) was determined as the y intercept of the equation regressing log height above the substrate against the measured flow speed. Regression equations generated for repeated measures in slow (3.8 cm/sec) and fast (14.4 cm/sec) flows produced correlation coefficients, $r^2 \geq 0.993$. The z_0 values calculated from regressions differed by $\leq 11\%$ between trials, indicating the bed form remained uniform during the course of this study.

Roughness Reynolds number was determined as:

$$Re_* = \frac{u_* D}{\nu} \quad (2)$$

where D is the height of the roughness elements (e.g., the diameter of the sand grains forming the bed), and ν is the kinematic viscosity of the fluid (0.01 cm²/sec). Based on the measured diameter of the sand grains, we used a value of 351 μm for D . We estimated the thickness of the viscous sublayer for each flow regime by reworking equation 2 and solving for D , setting $Re_* = 6$. Trials were conducted at two free-stream (U_∞) velocities, 3.8 cm/sec (slow flow) and 14.4 cm/sec (fast flow). A summary of the hydrodynamic measures for the two flow regimes is shown in Table 1.

Odor Plume Generation

To simulate a biologically relevant odor plume, a chemical tracer (dopamine) was introduced into the flow through the excurrent siphon of a model clam. The clam was designed using principles and procedures developed by

TABLE 1. SUMMARY OF HYDRODYNAMIC PARAMETERS FOR FLOW REGIMES USE IN EXPERIMENTS

	Fast flow (14.4 cm/sec)	Slow flow (3.8 cm/sec)
Roughness Reynolds number (Re_*)	3.56	1.26
Frictional velocity (μ_*)	1.22 cm/sec	0.36 cm/sec
Viscous sublayer thickness	0.042 cm ^a	0.207 cm ^a

^aThese values are only approximate estimates of the true layer thickness.

Monismith et al. (1990). The scale of our model bivalve (physical size and pumping rate) corresponds to a small hard clam, *Mercenaria mercenaria*, common in estuaries along the Atlantic and Gulf coasts of the United States. The model clam was created as a pair of tubes with their tips protruding vertically 5 mm above the substrate, simulating excurrent (3.1 mm ID) and incurrent (4.7 mm ID) siphons of a living animal. The excurrent tube was placed on the downstream side. Both the diameters and positions of the siphonal tubes were set, based on in situ observations and measurements of clams as part of another study (Weissburg and Zimmer-Faust, 1993).

The excurrent flow was supplied from a small, constant-head tank while the incurrent flow was taken by gravity feed from the flume (see methods section in Monismith et al., 1990). To ensure equality of the incurrent and excurrent flow rates, we continuously monitored these flows with inline flowmeters. Experiments were performed with a flow rate of 0.5 ml/sec through the siphon pair, with the Reynolds number of the siphon jet ≈ 170 . At this Reynolds number, the jet is laminar at the point where it leaves the excurrent siphon (List, 1982; Monismith et al., 1990).

As a frame of reference, we define the spatial coordinates of the siphon as $x = y = 0$, $z = 0.5$ cm. The x dimension is the downstream axis and y dimension is the cross-stream axis. The z dimension is oriented vertically into the water column with $z = 0$ defined as the boundary between the bed and the water column. Chemical recordings were made at $y = 0$, $x = 10, 25, 31, 50, 75, 100$ cm. At each of these six sites, chemical measurements were repeated at z -axis heights of $<1, 8, \text{ and } 50$ mm. The heights corresponded roughly to positions within the viscous sublayer, log layer and log-deficit layer, respectively, as verified by theoretical calculations and repeated vertical profile measurements. Chemical recordings were made at 10 Hz for 3 min at each of the 18 different positions.

Electrochemical Microelectrodes

Since the introduction of microelectrochemical techniques to aquatic applications, it has become possible to quantify chemical distributions at very small spatial scales and with high temporal resolution (Moore et al., 1989). The spatial and temporal scales required in quantifying chemical stimulus distributions relevant to aquatic organisms can be estimated from behavioral and electrophysiological studies. For instance, most arthropods orient to chemical signals using sensory input from antennae or antennules (insects, Kennedy, 1986; crustaceans, Reeder and Ache, 1980; Devine and Atema, 1982). These appendages usually have small hairs or sensilla that are permeable to odors and contain the dendrites for the primary receptor cells (Ghiradella et al., 1968; Laverack, 1988). To match the spatial sampling area associated with a single sensillum (30 μm diam-

eter and 1000 μm length), we chose electrochemical electrodes with diameters of 100–150 μm . In contrast to spatial scales, the temporal sampling scales for chemoreceptor cells are not well understood and must be estimated from flicker fusion and receptor adaptation studies. Neurons, both peripheral and CNS, can give distinct responses to odor pulses as fast as 10 Hz in two moth species (Kaissling et al., 1987; Christensen and Hildebrand, 1988). Similar studies in the American lobster, *Homarus americanus* have found peripheral chemoreceptor cells that can follow 4-Hz pulses (Gomez et al., 1992) and begin to adapt in 500 msec (Voigt and Atema, 1990). From these studies, we can estimate a temporal sampling scale between 100 and 500 msec. In addition, frequency spectra of aquatic odor signals measured at sampling rates of 10, 25, and 200 Hz (Moore and Atema, 1988, 1991; Atema et al., 1991) have shown that most of the odor signal fluctuations lie below 10 Hz. Thus, a sampling rate of 10 Hz will provide enough resolution to capture signal features most relevant to aquatic chemoreceptors.

We used a single graphite-epoxy capillary electrode (Gerhardt et al., 1984) with a tip diameter of 150 μm . The sampling area is determined by the exposed carbon-epoxy surface area (Adams, 1969; Gerhardt et al., 1987). Recordings were made at a sampling rate of 10 Hz using the IVEC-5 (In Vivo Electrochemistry Computer System; Medical Systems Corp., Greenvale, New York). Each 100-msec epoch for the 10 Hz sampling rate is composed of a 50-msec epoch at ± 0.55 V (oxidation) followed by a 50 msec epoch at 0.0 V (reduction). The recording electrodes were sampled every 50 msec; analog-to-digital conversions of the samples occurred at 4 KHz, and data were averaged for the 50-msec time epoch. Further details of recording and digitizing are explained elsewhere (Moore et al., 1989).

Electrodes were calibrated in solutions of dopamine prepared in filtered seawater and exhibited excellent linearity over a concentration range of 0.5–100 μM (correlation coefficient; $r^2 > 0.96$). We used a source concentration of 2 mM dopamine (and 0.1 mM ascorbic acid as an antioxidant).

The effect of flow on concentration measured by a sensor was tested by placing an electrode in known concentration solutions at different flow velocities. The tip of the electrode was precisely positioned, then sealed in the center of tygon tubing (0.317 cm ID), which was connected to a calibrated syringe drive. The tubing was long enough (4 m) to ensure a fully developed boundary layer for flow before contact was made between an injected solution and the sensor tip. A 5 μM dopamine solution was driven past the sensor at six flow velocities ranging from 1.6 cm/sec to 10.1 cm/sec. Flow velocity at the sensor tip was calculated as $2 \times$ the mean averaged over the entire cross-sectional area of the tube, as required for flow in a cylindrical pipe. The concentration measured by the electrodes changes linearly with flow speed ($r^2 = 0.96$). The slope of this relationship for the GEC electrodes is 0.20. Thus, a 5 μM concentration in a

still solution is measured as $5.8 \mu\text{M}$ at 3.8 cm/sec and $7.8 \mu\text{M}$ at 14.4 cm/sec . This relationship is consistent with the performance of microchemical sensors, which behave as though they are in stirred solutions (Adams, 1969; Galus et al., 1982). This increase is due to greater chemical flux across the sensor per unit time and not due to any changes in the response properties of the electrode. For the sake of simplicity, we use the term "concentration" to describe the calibrated signal from the electrodes. A more accurate description in flowing systems may be "molecular encounters per unit time." In this way, the electrodes and chemoreceptor cells in a flowing environment measure chemical signals in an identical manner.

Flow Visualization

To visualize the behavior of the plume generated by the model clam, we mixed a dilute solution of fluorescein (0.01% by weight) into the stimulus fluid. At these concentrations, the dye was neutrally buoyant. We used a halogen slit light source to illuminate the dye as the jet was ejected from the excurrent siphon. Images of the excurrent plumes were video-recorded from the side of the flume for 1 min at a series of positions at known distances from the origin, providing a visual record of the plume extending 100 cm downstream. The field of view was either $5 \times 5 \text{ cm}$ ($< 10 \text{ cm}$ downstream from source) or $15 \times 15 \text{ cm}$ ($> 10 \text{ cm}$ downstream). After each recording sequence, vertical and horizontal scales were filmed for later determinations of the spatial coordinates of the plume and for transformation to coordinates established above. Images of the plume were replayed through a motion analysis system in order to determine the trajectory of the plume. The center of mass was estimated visually along the x axis at 2.5-mm intervals for the first 10 cm, and thereafter at 5-cm intervals. At each position along the x axis, average plume position was generated by using the center of mass coordinates on 30 alternate video frames.

Data and Statistical Analysis and Definition of Terms

All measurements were converted from computer to micromolar concentrations of dopamine using the calibration factor determined for the electrode in static solutions. Odor profile parameters were extracted from the calibrated odor plume signals based on the definitions set forth in Moore and Atema (1991). While many statistical measures and signal analysis procedures could be used to analyze the signals presented here, we chose those parameters and analysis procedures that are more relevant to neuronal detection and coding of chemical signals. Computer simulations (Moore and Atema, 1988; Moore et al., 1992) and electrophysiological studies (Gomez et al., 1992; Borroni and Atema, 1988, 1989) have demonstrated that stimulus parameters such as pulse slope, height, length, and off time are important for determining the temporal response char-

acteristics of primary chemoreceptor cells. In addition, statistical measures taken over the whole recording period, such as mean level of concentration over 3 min may be poor indicators of the information available to animals making decisions in seconds based on sensory information integrated over milliseconds (Elkinton et al., 1984). Thus, the analysis we use is especially relevant to the biological detection of chemical signals by chemoreceptor cells. The definitions of plume parameters (based on Moore and Atema, 1991) used for our analysis are reviewed here in brief.

Odor Profile: a plot of concentration versus time that shows the concentration fluctuations at a single sampling site (Figures 2 and 3).

Odor Burst: within an odor profile there are periods with and without odor. Periods during which the odor concentration is detectable by the sensor are called odor bursts. A burst ends when the concentration drops below detectable levels (Figure 2).

Odor Pulse: within an odor burst, there may be multiple peaks and valleys of odor concentration (asterisks in Figure 2). Each of these peaks is considered a separate odor pulse only when the valley between the pulses falls to a value that is below 30% of the first pulse height. Odor pulses can be characterized by *pulse height*, highest concentration obtained during the pulse; *pulse length*,

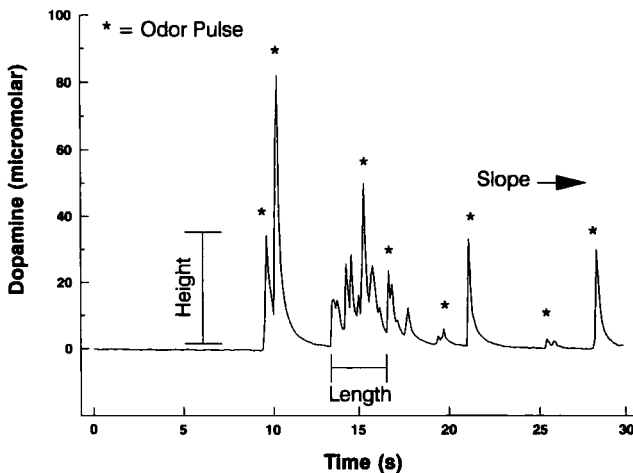


FIG. 2. Thirty-second temporal profile of dopamine concentrations at the slow flow velocity (3.8 cm/sec) demonstrating pulse parameters analyzed. Pulse height was measured against background level and pulse length was time from beginning to ending of odor pulse. Pulse slope was maximum slope on the rising side of the peak. Sampling site was located at $x = 31$ cm, $z = 50$ mm.

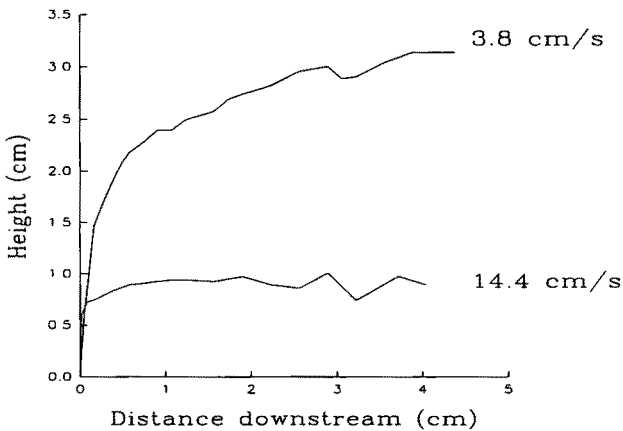


FIG. 3. Center of mass calculations showing differences in odor plume height at the two flow speeds (3.8 and 14.4 cm/sec). At the slower flow speed, the odor plume climbed to a higher level than at the faster flow speed during the first 5 cm downstream. Details on center of mass calculations are given in the text.

duration of pulse; and *pulse onset slope*, maximum value of rising slope of pulse.

Based on Moore and Atema (1988, 1991) further statistical analysis used pulse height and pulse slope as potential indicators of directional information. Differences in mean values for pulse height and slope were tested using an a posteriori statistic: Tukey test after an ANOVA (Zar, 1984). For spatial representation of probability distributions, pulse height (μM) and pulse slope ($\mu\text{M}/\text{sec}$) were grouped in five log-step bins (0.1–0.9, 1–9, 10–90, 100–900, 1000–9000). Probability distributions of pulse height and slope were calculated dividing the number of occurrences within a log-step bin by the total number of pulses encountered at that particular sampling site. A χ^2 analysis (SPSS, cross-tabs, SPSS Inc., Chicago, Illinois) of the categorized probability distributions was used to examine the effect and interaction of flow speed, height above substrate, and distance downstream on the probability distributions of pulse height and slope.

RESULTS

Qualitative Description of Odor Plumes

The trajectories of the odor plumes were clearly different at the two free stream velocities (Figure 3). The plume at 3.8 cm/sec rose to greater height and bent parallel to the substrate at a greater distance downstream than the plume

at 14.4 cm/sec. The plume at 3.8 cm/sec showed evidence of turbulent boundary layer flow, generating ring vortices within the first 2 cm of the origin. Although eddies occasionally contacted the substrate, the plume never reattached to the bottom, and the center of mass continued to rise as it traveled downstream. The plume at 14.4 cm/sec exhibited greater effects of turbulence than the jet at 3.8 cm/sec. At 14.4 cm/sec, the plume trajectory was unsteady, oscillating vertically in response to turbulent fluctuations in the flow. This was often associated with the rapid generation of large-scale coherent structures that were subsequently shed, generally within 5 cm of the origin. The plume reattached to the bottom within the first 5 cm and maintained contact at least 100 cm downstream. Although the effects of turbulence presumably caused dispersion and elevation of the plume's center of mass, the greater range of eddy sizes caused an increase in dilution of the dye stream. This rendered the top edge of the plume difficult to see and produced an apparent leveling off of the plume trajectory as it traveled downstream.

Although the odor source was constantly emitting dopamine, odor profiles were heterogeneous in time (Figure 4). Odor profiles were characterized by both odor bursts and pulses. In the present study, bursts frequently lasted from 5 to 10 sec (Figure 2, 13–18 sec), while pulses lasted between 0.5 and 6 sec (Figure 2, 21–22 sec). Peak odor concentrations during the pulse were diluted about 20 times as compared to the initial source concentration; i.e., from 2 mM to 100 μ M.

Effect of Flow Regime on Plume Parameters

Number of Pulses. The faster flow velocity had a greater number of pulses at most of the sites measured (14 of 18 sites) than the slow flow speed (Figure 5). This is consistent with greater turbulence generated at 14.4 cm/sec (indicated by the higher friction velocity). Only the $z = 50$ mm, $x = 10, 25, 31,$ and 100 cm sites at the slow velocity had more pulses than the corresponding fast velocity sites. At all of the $z = 1$ and 8 mm sites, the fast velocity exhibited larger numbers of pulses than the corresponding sites at the slow velocity.

Within the fast velocity, all of the $z = 8$ mm sites consistently showed a greater number of pulses than either the $z = 1$ or 50 mm sites. (Figure 5A, gray bars). This ranged from 90 ($z = 8, x = 25$) to 157 pulses ($z = 8, x = 10$). There was no consistent association of the number of pulses versus downstream distance from the odor source within the $z = 1, 8$ mm sites. The $z = 50$ mm depth showed an increase in the number of pulses as distance from the odor source increased. This trend was consistent except for the $x = 100$ cm site, which showed fewer pulses than the previous ($x = 75$ cm) site.

For the slow flow velocity, the $z = 50$ mm distance showed a greater number of pulses than the $z = 1$ and 8 mm sites (except the $x = 75$ cm site;

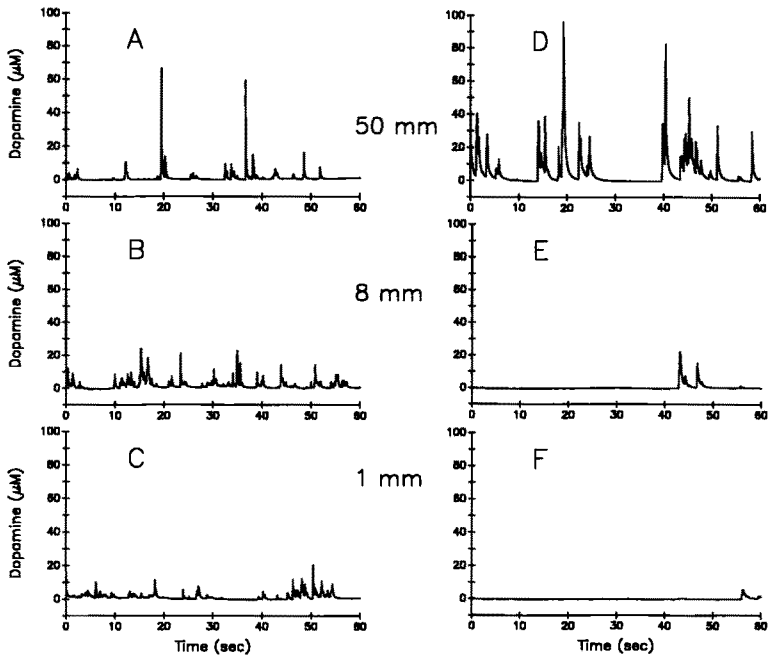


FIG. 4. One-minute dopamine concentration profiles recorded at the $x = 31$ cm cross-sectional plane. Profiles are from the fast flow velocity (14.4 cm/sec): $z = 50$ mm (A), $z = 8$ mm (B), $z = 1$ mm (C) and slow flow velocity (3.8 cm/sec): $z = 50$ mm (D), $z = 8$ mm (E), $z = 1$ mm (F). One-minute segments were chosen to show the most intense period of odor fluctuations in the 3-minute record.

Figure 5B, open bars). None of these sites had a consistent relationship between number of pulses and downstream distance from the odor source.

Pulse Height and Slope. At the fast flow speed the odor plume had a lower center of mass, which is reflected in higher mean pulse heights at 8 and 1 mm as compared to 50 mm (Figure 6). The mean pulse height was significantly higher ($P < 0.01$) at the 10-cm site than at the other distances at both the 8- and 1-mm height above from the substrate. The mean pulse height decreased with increasing distance from the odor source, although this change was not significant. It was only when the plume traveled 30 cm downstream that it dispersed vertically enough so that relatively large pulse heights are encountered at the 50 mm height. The maximum mean pulse height was reached at 30 cm downstream from the odor source, and this pulse height was significantly higher than only the 10-, 75-, and 100-cm sites ($P < 0.01$; Figure 6A). Once the

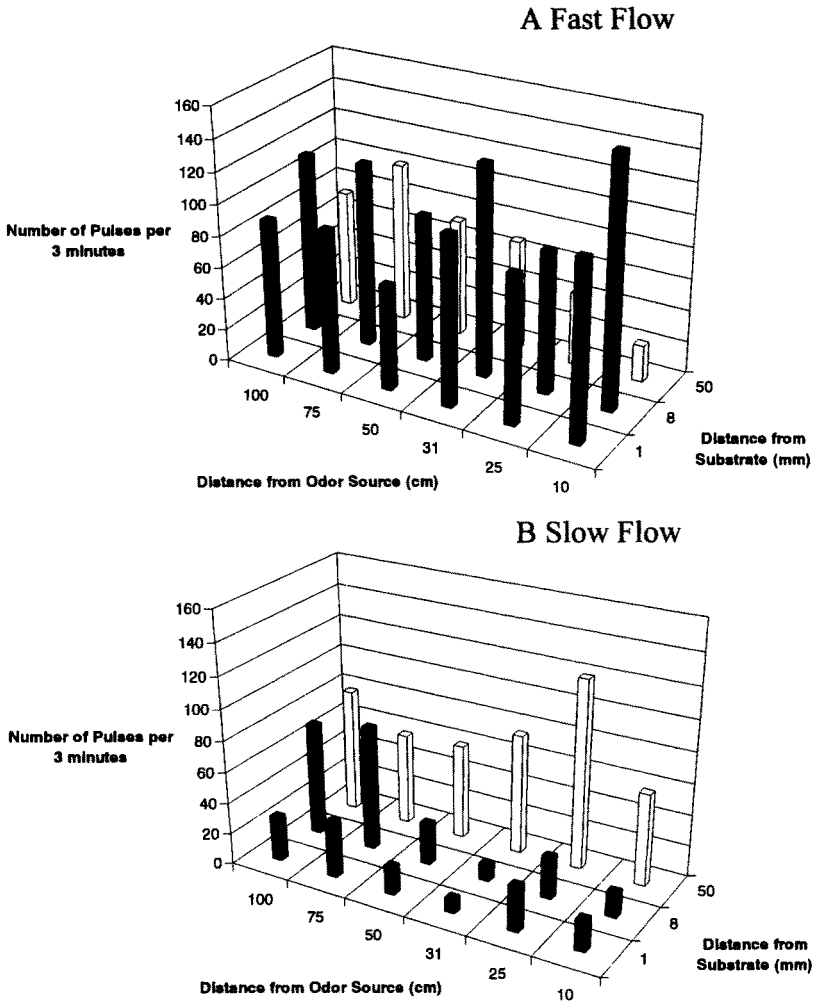


FIG. 5. Number of pulses within the 3-min odor profiles for the fast flow (A) and slow flow (B) conditions. Shaded bars represent distance up from substrate: 50 mm (open), 8 mm (gray), 1 mm (black).

maximum was reached, the pulse heights decreased with increasing distance downstream.

The distribution of pulse heights at the slow speed showed a different spatial pattern than those seen at the fast speed (Figure 6D, E, and F), since the plume heads parallel to the substrate rather high in the water column. The largest pulse

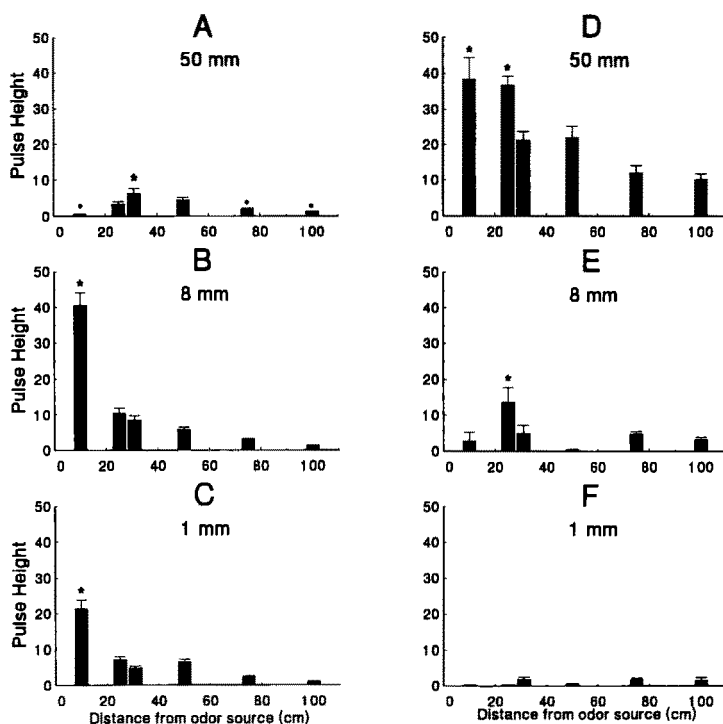


FIG. 6. Mean (\pm SEM) pulse height (in μM values) taken over the 3-min recording period for the fast flow (A, $z = 50$ mm; B, $z = 8$ mm; C, $z = 1$ mm) and the slow flow (D, $z = 50$ mm; E, $z = 8$ mm; F, $z = 1$ mm) conditions. Asterisks represent pulse heights that are significantly different from all means within any one graph, except A where an asterisked mean is different only from means with solid circles above them. Sample sizes for means are the same as in Figure 5.

heights were measured at the highest distance (50 mm) up from the substrate (Figure 6D). At this location, the pulse heights at both the $x = 10$ and 25 cm sites were significantly larger than at any other downstream site (Tukey-Kramer, $P < 0.01$). Although the pulse heights decreased with increasing distance from the odor source, this decrease is less than that measured at the higher flow velocity. The lower level of turbulence seen at the slow (versus the fast) flow velocity (see Table 1) had a lesser effect on dispersing and mixing the odor plume as it traveled downstream. Conversely, the high level of turbulence at the high flow velocity served to break up the larger patches of odor into smaller and more discrete odor pulses. This resulted in lower mean pulse height within the main axis of the odor plume at the slow flow as compared to the fast flow

(compare Figure 6B with 6D, sites 25, 30, 50, 75, and 100 cm). The spatial distribution of mean pulse slopes were very similar to the distributions seen for mean pulse height and thus were not shown.

Although the pulse heights were higher at the 50-mm sampling site and at the slow flow, the overall slopes compared to their heights were lower than for the pulses encountered at the faster flow. Higher slopes may just be a consequence of higher pulse height when sampling over a constant time interval. The slope-to-height ratio (Table 2) is an indication of the steepness of the onset of odor within a pulse and is independent of the absolute pulse height. This parameter allows for comparison of onset slopes of pulses of different heights (Figure 6A and D). It becomes evident when comparing the slope-to-height ratios for the fast and slow flows that the odor pulses within the fast flow are more discrete and tightly packed. Most of the odor pulses encountered in the fast flow had higher ratios than the corresponding sampling sites in the slow flow (Tukey-Kramer, $P < 0.01$; all sites were significant except for $z = 50, x = 25, 100$; $z = 8, x = 25, 50$; $z = 1, x = 10$). This is particularly evident at the 50-mm sampling height. While the slow flow has considerably higher mean pulse heights (sometimes 20 times larger, compare Figure 6D and 6A), the fast flow has larger slope-to-height ratios.

The probability distributions of pulse slopes from the fast flow velocity (14.4 cm/sec) are seen in Figure 7. All three heights from the substrate showed similar distributions far from the odor source, i.e., 75 and 100 cm. Differences in distributions increased near the odor source, i.e., 10 and 25 cm (χ^2 analysis, $P < 0.001$). The most consistent change with distance was seen in the probability distribution at the $z = 1$ mm height (χ^2 analysis, $P < 0.001$). Far away from the source (100 cm), most of the pulse slopes (80%) occurred in the 1-9

TABLE 2. MEAN (\pm SEM) SLOPE-TO-HEIGHT RATIO AS FUNCTIONS OF FLOW SPEED AND DISTANCE DOWNSTREAM

Height (mm) above substrate	Downstream distance					
	10 cm	25 cm	31 cm	50 cm	75 cm	100 cm
Fast Flow						
50	6.5(0.5)	6.3(0.4)	7.4(0.3)	7.7(0.3)	6.9(0.2)	7.2(0.3)
8	6.7(0.2)	5.6(0.3)	6.2(0.2)	5.6(0.2)	5.5(0.2)	6.1(0.2)
< 1	5.5(0.2)	5.9(0.3)	6.7(0.3)	5.4(0.2)	5.8(0.2)	6.1(0.3)
Slow flow						
50	4.8(0.4)	6.2(0.2)	5.6(0.3)	6.5(0.3)	7.0(0.4)	7.3(0.4)
8	5.6(0.6)	5.7(0.6)	4.8(0.7)	5.5(0.4)	6.0(0.4)	4.5(0.3)
< 1	6.0(0.4)	5.0(0.2)	3.0(0.7)	5.0(0.5)	4.3(0.3)	5.1(0.5)

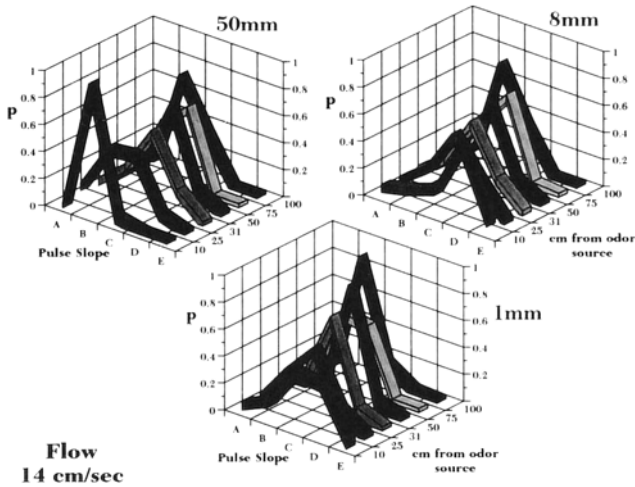


FIG. 7. Probability distributions of pulse slope taken in the fast flow (14.4 cm/sec) at the 50-, 8-, and 1-mm distances from the substrate. Probability values were calculated for five different bin sizes: (A) 0.1–0.9, (B) 1–9, (C) 10–90, (D) 100–900, (E) 1000–9000 $\mu\text{M}/\text{sec}$.

$\mu\text{M}/\text{sec}$ bin. This range of possible pulse slopes gradually increased to the 10 cm site. Both the 50 and 8 mm heights showed this same trend although not as dramatically.

Each of the probability distributions at the slow speed (Figure 8) were different from the corresponding distributions at the fast speed (Figure 7; χ^2 analysis, $P < 0.005$). The highest pulse slopes were seen in the probability distributions at $z = 50$ mm height (Figure 8). The $z = 8$ mm height contained a mixture of pulse slope values and had no consistent change in distributions with distance from odor source. The $z = 1$ mm height had shallow slopes at all distances except at the $x = 25$ cm. None of these distributions had any association with downstream distance such as that seen at the fast flow speed.

The probability distributions for pulse height at 14.4 cm/sec showed no consistent trend with distance at any of the heights along the z axis (Figure 9). All three heights ($z = 1, 8, 50$ mm) had similar distributions at all downstream distances from the odor source except at the $x = 10$ cm, where at the $z = 50$ mm site, almost all of the pulse heights were 0.1–0.9 μM (χ^2 analysis, $P < 0.001$). In comparison, at the $z = 8$ and 1 mm sites, the majority of the pulse heights were in the 10–90 μM range.

The probability distributions for pulse height at the slow flow speed were shifted to the lower pulse heights at the $z = 8$ and 1 mm heights (Figure 10;

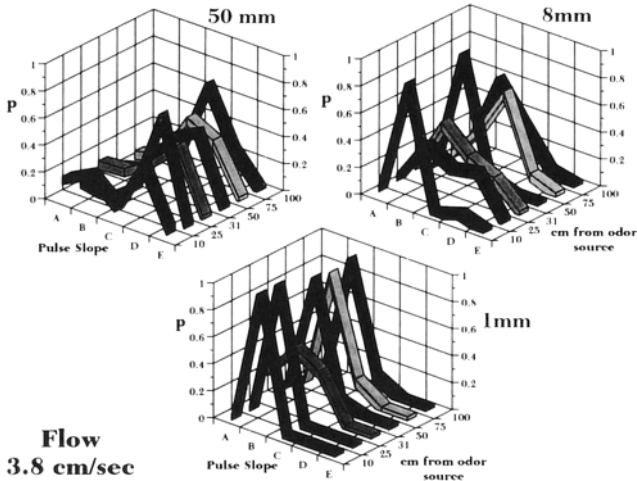


FIG. 8. Probability distributions of pulse slope taken in the slow flow (3.8 cm/sec) at the 50-, 8-, and 1-mm distances from the substrate. Probability values were calculated for five different bin sizes: (A) 0.1-0.9, (B) 1-9, (C) 10-90, (D) 100-900, (E) 1000-9000 $\mu\text{M}/\text{sec}$.

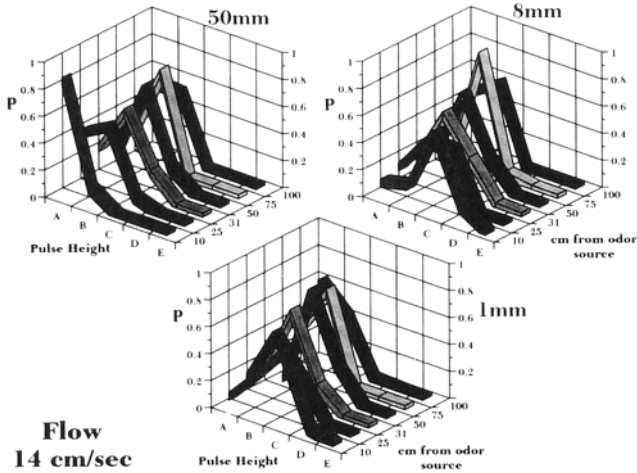


FIG. 9. Probability distributions of pulse height taken in the fast flow (14.4 cm/sec) at the 50-, 8-, and 1-mm distances from the substrates. Probability values were calculated for five different bin sizes: (A) 0.1-0.9, (B) 1-9, (C) 10-90, (D) 100-900, (E) 1000-9000 μM .

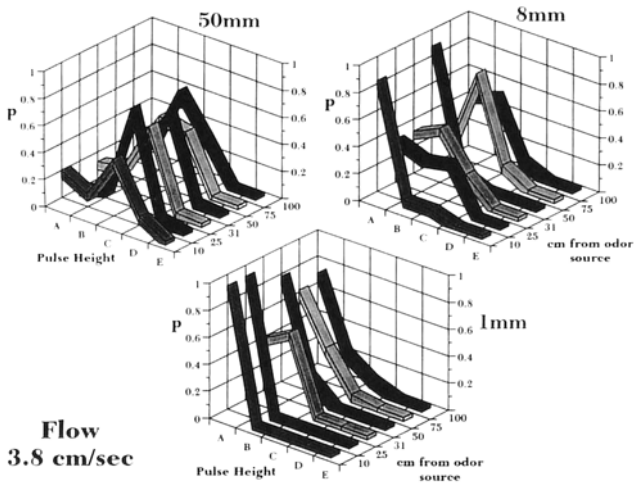


FIG. 10. Probability distributions of pulse height taken in the slow flow (3.8 cm/sec) at the 50-, 8-, and 1-mm distances from the substrates. Probability values were calculated for five different bin sizes: (A) 0.1–0.9, (B) 1–9, (C) 10–90, (D) 100–900, (E) 1000–9000 μM .

χ^2 analysis, $P < 0.001$). The majority of pulses had heights of 1–9 and 0.1–0.9 μM . The distributions for the $z = 50$ mm height (slow flow) were higher than those for the fast flow. Most of the pulses in this plane had heights of 10–90 μM .

DISCUSSION

These studies demonstrate three major consequences of different flow velocities in the distribution of chemicals. First, slower flow velocities allow the initial energy of the model clam excurrent to carry the dopamine farther into the water column before the carrier flow begins to transport the chemical down-current. As a result of this, the main axis of the plume will be located higher in the water column at slower flow velocities than at faster velocities (Figure 3). The main axis of an odor plume contains the most odor pulses and exhibits the largest fluctuations in concentration (compare Figure 4D with E and F; Figure 5). If animals are relying on the main axis of the plume as the major source of directional information during orientation, they must switch sampling and/or search strategies depending upon the flow conditions.

Secondly, there is a general relationship between plume microstructure and the magnitude and degree of penetrance of turbulence into the boundary layer.

Increased turbulence serves both to disperse odors and to distribute odor molecules into smaller and more discrete patches (Figure 6). Conversely, less turbulent flows result in greater average odor concentrations and more uniform distribution of odor further downstream from the source (Figure 6). Thus, within the main axis of the plume, average pulse height tended to show larger decreases at the high flow velocity ($U_\infty = 14.4$ cm/sec) than at the low flow velocity ($U_\infty = 3.8$ cm/sec). The plumes at the high flow velocity also exhibited a greater number of pulses and higher pulse slopes relative to the plume generated at the slower flow (Figure 5; Table 2). The effect of increasing u_* and Re_* , and thus boundary layer turbulence, is particularly clear when examining the distribution of pulse slopes and heights close to the substrate. At high flow, there is an increase in boundary layer turbulence close to the substrate which entrains odors in eddy structures, transporting them closer to the bed (Table 1). This results in a greater number of discrete odor patches and therefore higher odor concentrations and faster onset slopes, within 1 mm of the bottom in faster flows.

Thirdly, increased turbulence generally resulted in a more predictable relationship between microscale plume structure and distance to the odor source. At 14.4 cm/sec plumes remained more patchy as they were advected downstream as compared to the slow flow velocity. These smaller and more discrete patches have higher concentration gradients between patch-nonpatch boundaries. Thus, in general, odor pulses have higher slope-to-height ratios at higher flow velocities. At the slower speed, odor patches take a longer time to move downcurrent. This increase in transport time is correlated with a smoothing of the concentration gradient at patch boundaries, resulting in decreased slope and slope-to-height values. Consequently, the distribution of pulse slopes, and to a lesser extent pulse heights, both tended to show a correlation with downstream distance from the odor source within all boundary layer regions at the higher flow speed. At the slow flow velocity, there was rarely any relationship between distance and plume microstructure. Due to the small degree of turbulent velocity fluctuations penetrating within the viscous sublayer, only pulse slopes within the log-deficit layer (i.e., $z \approx 50$ mm) show any correlation with distance to the odor source, and even here the relationship is not very robust. Thus, turbulence not only alters plume microstructure, but also the spatial information content potentially contained within regions of the boundary layer.

Turbulence creates large-scale eddies that transfer their energy to successively smaller eddies until the energy is dissipated as heat. This cascade of eddies (Kolmogorov scale) has a lower size limit below which molecular diffusion is the predominant transport mechanism. The spatial range of eddies is important because it is the interaction of the eddy size and plume size that contributes to the size and length of concentration fluctuations within the odor plume (Aylor, 1976; Aylor et al., 1976; Miksad and Kittredge, 1979). When

the plume or odor patch diameter is smaller than the smallest eddies, the eddies cause the plume/patch to meander as a whole. As the plume/patch expands to match the scale of eddies present, the plume/patch is broken into smaller more discrete patches of odor. The final stage of plume growth occurs when the plume/patch expands to sizes larger than the largest eddies. At this point, eddies begin to redistribute the odor within single patches and begin to homogenize the odor between patches. Other factors, such as shear, may also play a role in smoothing patch-nonpatch boundaries (Tennekes and Lumley, 1972). Higher levels of turbulence will have smaller minimum eddy sizes and, thus, smaller and more discrete odor patches. Lower levels of turbulence will not have as many small eddies, and odor patches will tend to be larger and greater in concentration (Figures 4 and 6). The theoretical minimum eddy size (η) can be calculated from equation 3 (Tennekes and Lumley, 1972):

$$\eta = (\kappa Z \nu^3 / u_*^3)^{1/4} \quad (3)$$

This yields a minimum eddy size of 809 μm for 3.8 cm/sec and 323 μm for 14.4 cm/sec. The smaller theoretical minimum eddy size at the higher flow corresponds to the differences in the size and number of small odor patches seen between the two flow rates. The minimum concentration fluctuation (η_c) can then be determined from equation 4:

$$\eta_c = \eta(D/\nu)^{1/2} \quad (4)$$

where $D = 10^{-5} \text{ cm}^2/\text{sec}$ (molecular diffusion coefficient for dopamine in seawater). Applying equation 4, we find that $\eta_c \approx 25 \mu\text{m}$ for 3.8 cm/sec and 10 μm for 14.4 cm/sec.

Previous studies have begun to explore microscale properties of chemical distributions within odor plumes. These properties may contain information valuable to animals and potentially guide their orientation towards distant sources of odor (Murlis and Jones, 1981; Moore and Atema, 1988, 1991; Zimmer-Faust et al., 1988; Murlis et al., 1991). These studies have concentrated on pulse height, slope, length, and intermittency as possible sources of directional information. Our current study has found that the spatial distribution of these parameters is highly dependent upon the magnitude of turbulence present, which can be effected by hydrodynamic forces. Thus, any spatial information contained within the plume structure will vary in different flows. Pulse slope decreased consistently with downstream distance at 14.4 cm/sec, and could potentially give orienting animals directional information within a plume. Since the most consistent spatial information is located in different heights above the substrate in different hydrodynamic conditions, animals using these parameters for directional information during orientation may modify their sampling, searching, and/or locomotor strategies to fit the appropriate flow conditions. In future behavioral studies, it will have to be determined if changes in locomotor output represent

a switch in sampling strategies or the same strategy where different sensory input alters locomotory output.

Two recent behavioral studies on benthic decapod crustaceans illustrate these ideas (Scholz and Atema, 1991; Weissburg and Zimmer-Faust, 1993). These studies both used animals normally found within benthic boundary layer conditions and that rely heavily on chemical signals for a number of different behaviors. In both of these studies, there was a linkage between locomotory performance, chemical signal structure, and hydrodynamic conditions. These studies could indicate a changing of the overall search strategy of the animal. Conversely, the change in locomotor output may only represent the response to the different spatial distribution of chemicals rather than a change in search behavior. These changes in behavior have been shown for terrestrial insects (Baker et al., 1984) and are thought to be controlled by both the local wind direction and presence or absence of pheromone (David et al., 1982).

Our results have demonstrated that in different turbulent flow regimes chemical signal distribution will change considerably near a solid surface. It has been demonstrated that the morphology of appendages influences the hydrodynamics of flow around and through them (Rubenstein and Koehl, 1977; Cheer and Koehl, 1987), and this in turn will affect the structure of chemical signals near receptor cells (Moore et al., 1991; Gleeson et al., 1993). Our present study shows that chemosensory appendages located within the viscous sublayer will receive slow and near-continuous signals, whereas appendages higher up in the flow will receive faster and more variable signals. The morphology of a chemosensory appendage and the sampling behavior may be correlated with the hydrodynamics of the flow regime in which they are normally located. Thus, the morphological influence on fluid flow and sampling behaviors of different appendages may be adapted to the different types of chemical signals in their relative microenvironments (Moore et al., 1991).

In summary, higher turbulence results in smaller and more discrete odor patches that arrive more frequently. These patches have very high slopes associated with the patch-nonpatch boundary. Conversely, lower turbulence results in large, slowly rising, high concentration odor patches that occur less frequently. Aquatic animals living in benthic environments therefore may have specific search strategies or locomotory patterns maximizing their ability to navigate towards a source of odor. These strategies would need to be sensitive to different hydrodynamic regimes and changing microscale stimulus conditions.

Acknowledgments—The authors thank Dr. Jelle Atema for critically reviewing an earlier version of this manuscript. Our work was supported by NIH grants AG00441 and AG06434 and NSF grant BNS-9110308 to G. A. G.; NSF grants R11-8996152, DIR-8954231, and IBN-922225 to R. Z. F.; and an ADMH Drug Abuse Training Fellowship (AA07464) to P. M.

REFERENCES

- ADAMS, R.N. 1969. *Electrochemistry at Solid Electrodes*. Marcel Dekker, New York.
- ATEMA, J. 1985. Chemoreception in the sea: Adaptation of chemoreceptors and behavior to aquatic stimulus conditions. *Soc. Exp. Biol. Symp.* 39:387-423.
- ATEMA, J. 1988. Distribution of chemical stimuli, pp. 29-56, in J. Atema, A. N. Popper, R. R. Fay and W. N. Travalga (eds.). *Sensory Biology of Aquatic Animals*. Springer-Verlag, Berlin.
- ATEMA, J., MOORE, P.A., MADIN, L.P., and GERHARDT, G.A. 1991. Subnose-I: electrochemical tracking of odor plumes at 900 m beneath the ocean surface. *Mar. Ecol. Prog. Ser.* 74:303-306.
- AYLOR, D.E. 1976. Estimating peak concentrations of pheromones in the forest, pp. 177-188, in J.E. Anderson and M.K. Kaya (eds.). *Perspectives in Forest Entomology*. Academic Press, New York.
- AYLOR, D.E., PARLANGE, J.-Y., and GRANETT, J. 1976. Turbulent dispersion of disparlure in the forest and male gypsy moth response. *Environ. Entomol.* 10:211-218.
- BAKER, T.C., WILLIS, M.A., and PHELAN, P.L. 1984. Optomotor anemotaxis polarizes self-steered zigzagging in flying moths. *Physiol. Entomol.* 9:365-376.
- BELL, W. J., and TOBIN, T.R. 1982. Chemo-orientation. *Biol. Rev.* 57:219-260.
- BORRONI, P.F., and ATEMA, J. 1988. Adaptation in chemoreceptor cells I. Self-adapting backgrounds determine threshold and cause parallel shift of dose-response function. *J. Comp. Physiol. A.* 164:67-74.
- BORRONI, P.F., and ATEMA, J. 1989. Adaptation in chemoreceptor cells II. The effects of cross-adapting backgrounds depend on spectral tuning. *J. Comp. Physiol. A.* 165:669-677.
- CHEER, A.Y.L., and KOEHL, M.A.R. 1987. Paddles and rakes: fluid flow through bristled appendages of small organisms. *J. Theor. Biol.* 129:17-39.
- CHRISTENSEN, T.A., and HILDEBRAND, J.G. 1988. Frequency coding by central olfactory neurons in the sphinx moth, *Manduca sexta*. *Chem. Senses* 13:123-130.
- DAVID, C.T., KENNEDY, J.S., LUDLOW, A.R., PERRY, J.N., and WALL, C. 1982. A reappraisal of insect flight towards a distant, point source of wind borne odor. *J. Chem. Ecol.* 8:1207-1215.
- DENNY, M.W. 1988. *Biology and the Mechanics of the Wave-Swept Environment*. Princeton University Press, Princeton, New Jersey.
- DEVINE, D.V., and ATEMA, J. 1982. Function of chemoreceptor organs in spatial orientation of the lobster, *Homarus americanus*: Differences and overlap. *Biol. Bull.* 163:144-153.
- ELKINTON, J.S., CARDÉ, R.T., and MASON, C.J. 1984. Evaluation of time-average dispersion models for estimating pheromone concentration in a deciduous forest. *J. Chem. Ecol.* 10:1081-1108.
- ERTMAN, S.C., and JUMARS, P.A. 1988. Effects of bivalve siphonal currents on the settlement of inert particles and larvae. *J. Mar. Res.* 46:797-813.
- FISCHER, H.B., LIST, E.J., KOH, R.C.Y., IMBERGER, J., and BROOKS, J.H. 1979. *Mixing in Inland and Coastal Waters*. Academic Press, New York.
- GALUS, Z., SCHENK, J.O., and ADAMS, R.N. 1982. Electrochemical behavior of very small electrodes in solution. *J. Electroanal. Chem.* 135:1-11.
- GERHARDT, G.A., OKE, A.F., NAGY, G., MOGHADDAM, B., and ADAMS, R.N. 1984. Nafion-coated electrodes with high selectivity for CNS electrochemistry. *Brain Res.* 290:390-395.
- GERHARDT, G.A., ROSE, G.M., and HOFFER, B.J. 1987. In vivo electrochemical demonstration of potassium-evoked monoamine release from rat cerebellum. *Brain Res.* 413:327-335.
- GHIRADELLA, H., CASE, J.F., and CRONSHAW, J. 1968. Structure of aesthetascs in selected marine and terrestrial decapods: Chemoreceptor morphology and environment. *Am. Zool.* 8:603-621.
- GLEESON, R.A., CARR, W.E.S., and TRAPIDO-ROSENTHAL, H.G. 1993. Morphological characteristics facilitating stimulus access and removal in the olfactory organ of the spiny lobster, *Panulirus argus*: Insight from design. *Chem. Senses* 18:67-75.

- GOMEZ, G., VOIGT, R., and ATEMA, J. 1992. Frequency coding in chemoreceptor cells. *Chem Senses* 17:631-632.
- JOHNSEN, P.B., and TEETER, J.H. 1980. Spatial gradient detection of chemical cues by catfish. *J. Comp. Physiol. A* 140:95-99.
- KAISLING, K.E., ZACK-STRAUSSFELD, C., and RUMBO, E. 1987. Adaptation processes in insect olfactory receptors: mechanisms and behavioral significance, pp. 104-112, in S. Roper and J. Atema (eds.). *Olfaction and Taste IX*. New York Academy of Science, New York.
- KENNEDY, J.S. 1986. Some current issues in orientation to odour sources, pp. 11-25 in T.L. Payne, M.C. Birch, and C.E.J. Kennedy (eds.). *Mechanisms in Insect Olfaction*. Oxford University Press, New York, New York.
- LABARBERA, M., and VOGEL, S. 1976. An inexpensive thermistor flowmeter for aquatic biology. *Limnol. Oceanogr.* 21:750-756.
- LAVERACK, M.S. 1988. The diversity of chemoreceptors, pp. 287-312, in J. Atema, A.N., Popper, R.R. Fay, and W.N. Tavolga (eds.). *Sensory Biology of Aquatic Animals*. Springer-Verlag, Berlin.
- LIST, E.J. 1982. Turbulent jets and plumes. *Annu. Rev. Fluid Mech.* 14:189-212.
- MCLEESE, D.W. 1973. Orientation of lobsters (*Homarus americanus*) to odor. *J. Fish. Res. Board Can.* 30:838-840.
- MIKSID, R.W., and KITTREDGE, J. 1979. Pheromone aerial dispersion: A filament model. *14th Conf. Agric. and For. Met. Am. Met. Soc.* 1:238-243.
- MONISMITH, S.G., KOSEFF, J.R., THOMPSON, J.K., O'RIORDAN, C.A., and NEFF, H.M. 1990. A study of model bivalve siphonal currents. *Limnol. Oceanogr.* 35:680-696.
- MOORE, P.A., and ATEMA, J. 1988. A model of a temporal filter in chemoreception to extract directional information from a turbulent odor plume. *Biol. Bull.* 174:355-363.
- MOORE, P.A. and ATEMA, J. 1991. Spatial information in the three-dimensional fine structure of an aquatic odor plume. *Biol. Bull.* 181:408-418.
- MOORE, P.A., GERHARDT, G.A., and ATEMA, J. 1989. High resolution spatio-temporal analysis of aquatic chemical signals using microelectrochemical electrodes. *Chem. Senses* 14:829-840.
- MOORE, P.A., ATEMA, J., and GERHARDT, G.A. 1991. Fluid dynamics and microscale odor movement in the chemosensory appendages of the lobster, *Homarus americanus*. *Chem. Senses* 16:663-674.
- MOORE, P.A., ZIMMER-FAUST, R.K., BEMENT, S.L., WEISSBURG, M.J., PARRISH, M.J., and GERHARDT, G.A. 1992. Measurement of microscale patchiness in a turbulent aquatic odor plume using a semiconductor-based microprobe. *Biol. Bull.* 183:138-142.
- MURLIS, J., and JONES, C.D. 1981. Fine-scale structure of odour plumes in relation to insect orientation to distant pheromone and other attractant sources. *Physiol. Entomol.* 6:71-86.
- MURLIS, J., WILLIS, M.A., and CARDÉ, R.T. 1991. Odour signals: patterns in space and time, pp. 6-17, in K. Døving (eds.). *Proceedings of the Tenth International Symposium on Olfaction and Taste*, Graphic Communication System, Oslo.
- NOWELL, A.R.M., and JUMARS, P.A. 1984. Flow environments of aquatic benthos. *Annu. Rev. Ecol. Syst.* 15:303-328.
- NOWELL, A.R.M., and JUMARS, P.A. 1987. Flumes: Theoretical and experimental considerations for simulation of benthic environments. *Oceanogr. Mar. Biol. Annu. Rev.* 25:91-112.
- REEDER, P.B., and ACHE, B.W. 1980. Chemotaxis in the Florida spiny lobster, *Panulirus argus*. *Anim. Behav.* 28:831-839.
- RUBENSTEIN, D.I., and KOEHL, M.A.R. 1977. The mechanisms of filter feeding: Some theoretical considerations. *Am. Nat.* 111:981-994.
- SCHOLZ, N., and ATEMA, J. 1991. Effect of flow velocity on chemical signal dispersal and hermit crab orientation. *Chem. Senses* 16:577-578.

- TENNEKES, H., and LUMLEY, J.L. 1972. *A First Course in Turbulence*, MIT Press, Cambridge, Massachusetts, 300 pp.
- VOIGT, R., and ATEMA, J. 1990. Adaptation in chemoreceptor cells. III. Effects of cumulative adaptation. *J. Comp. Physiol. A.* 166:865-874.
- WEISSBURG, M.J., and ZIMMER-FAUST, R.K. 1993. Life and death in moving fluids: hydrodynamic effects on chemosensory-mediated predation. *Ecology.* 74:1428-1443.
- WESTERBERG, H. 1991. Properties of aquatic odour trails, pp. 45-65, in K. Døving (eds). *Proceedings of the Tenth International Symposium on Olfaction and Taste*, Graphic Communication System, Oslo.
- WRIGHT, L.D. 1989. Benthic boundary layers of estuarine and coastal environments. *Rev. Aquat. Sci.* 1:75-95.
- ZAR, J.H. 1984. *Biostatistical Analysis*, 2nd ed. Prentice Hall, Englewood Cliffs, New Jersey.
- ZIMMER-FAUST, R.K. 1989. The relationship between chemoreception and foraging behavior in crustaceans. *Limnol. Oceanogr.* 34:967-974.
- ZIMMER-FAUST, R.K., STANFILL, J.M., and COLLARD, S.B. III. 1988. A fast, multichannel fluorometer for investigating aquatic chemoreception and odor trails. *Limnol. Oceanogr.* 33:1586-1595.